

# Quark number densities at imaginary chemical potential in $N_f = 2$ lattice QCD with Wilson fermions and its model analyses

Junichi Takahashi,<sup>1,\*</sup> Hiroaki Kouno,<sup>2,†</sup> and Masanobu Yahiro<sup>1,‡</sup>

<sup>1</sup>*Department of Physics, Graduate School of Sciences, Kyushu University, Fukuoka 812-8581, Japan*

<sup>2</sup>*Department of Physics, Saga University, Saga 840-8502, Japan*

(Received 28 October 2014; published 8 January 2015)

We investigate the temperature ( $T$ ) dependence of quark number densities ( $n_q$ ) at imaginary and real chemical potential ( $\mu$ ) by using  $N_f = 2$  lattice QCD and the hadron resonance gas (HRG) model. Quark number densities are calculated at imaginary  $\mu$  with lattice QCD (LQCD) on an  $8^2 \times 16 \times 4$  lattice with the clover-improved  $N_f = 2$  Wilson fermion action and the renormalization-group-improved Iwasaki gauge action. The results are consistent with the previous results of the staggered-type quark action. The  $n_q$  obtained are extrapolated to real  $\mu$  by assuming the Fourier series for the confinement region and the polynomial series for the deconfinement region. The extrapolated results are consistent with the previous results of the Taylor expansion method for the reweighting factor. The upper bound  $(\mu/T)_{\max}$  of the region where the extrapolation is considered to be reliable is estimated for each temperature  $T$ . We test whether  $T$  dependence of nucleon and  $\Delta$ -resonance masses can be determined from LQCD data on  $n_q$  at imaginary  $\mu$  by using the HRG model. In the test calculation, nucleon and  $\Delta$ -resonance masses reduce by about 10% in the vicinity of the pseudocritical temperature.

DOI: 10.1103/PhysRevD.91.014501

PACS numbers: 11.15.Ha, 11.30.Fs, 12.38.Gc

## I. INTRODUCTION

There are many interesting topics on quantum chromodynamics (QCD) at high density. The observation [1] of a two-solar-mass neutron star has an impact on the equation of state (EOS) of dense matter and the QCD phase diagram at high density. The experiments of relativistic heavy-ion collisions, for example the beam energy scan experiments, are exploring QCD not only at finite temperature  $T$  but also at finite quark-chemical potential  $\mu$  [2,3]. Lattice QCD (LQCD) is the first-principle calculation to study QCD, but it has the serious sign problem at finite  $\mu$ .

In LQCD, the fermion determinant  $\det M(\mu/T)$  becomes complex for finite real  $\mu$ , because

$$(\det M(\mu/T))^* = \det M(-\mu^*/T) = \det M(-\mu/T). \quad (1)$$

This interferes with the use of Monte Carlo simulations based on the importance sampling. For this reason, several methods have been proposed to avoid the sign problem [4,5]. Very recently, the complex Langevin method [6–9] and the Lefschetz thimble theory [10,11] have attracted much attention as the method to go beyond  $\mu/T = 1$ .

One of the methods to avoid the sign problem is the imaginary- $\mu$  approach. For purely imaginary chemical potential  $\mu = i\mu_I$ , it is convenient to introduce the dimensionless chemical potential  $\theta = \mu_I/T$ . The first equality of Eq. (1) shows that the fermion determinant  $\det M(i\theta)$  is real

for imaginary  $\mu$ . This makes LQCD simulations feasible there. Observables at real  $\mu$  are extracted from those at imaginary  $\mu$  by assuming functional forms for the observables.

In the imaginary  $\mu$  region, QCD has two characteristic properties: one is the Roberge-Weiss (RW) periodicity and the other is the RW phase transition [12]. Figure 1 shows a schematic graph for the QCD phase diagram in the  $T - \theta$  plane. The QCD grand partition function  $Z(\theta)$  has a periodicity of  $2\pi/N_c$  in  $\theta$ ,

$$Z(\theta) = Z\left(\theta + \frac{2\pi k}{N_c}\right), \quad (2)$$

where  $N_c$  is the number of colors and  $k = 1, \dots, N_c$ . This is a remnant of  $\mathbb{Z}_{N_c}$  symmetry in pure gauge theory and is now called the RW periodicity. Meanwhile, the RW transition is the first-order phase transition appearing at  $T$  higher than some temperature  $T_{\text{RW}}$  and  $\theta = \pi/N_c$ . This transition line and its  $\mathbb{Z}_{N_c}$  images are plotted by the solid lines in Fig. 1. The point located at  $(T, \theta) = (T_{\text{RW}}, \pi/N_c)$  is called the RW end point. Meanwhile, the dashed line represents the transition line of confinement/deconfinement crossover. The pseudocritical temperature  $T_c(\theta)$  is a function of  $\theta$ , and the value at  $\theta = 0$  [13] is denoted by  $T_{c0}$ . As shown later,  $T_{\text{RW}}$  is located between  $1.08$  and  $1.20T_{c0}$ . The order parameter of the RW transition is a  $\mathcal{C}$ -odd quantity, such as the phase of the Polyakov loop or the quark number density [14], where  $\mathcal{C}$  means charge conjugation. The existence of the RW transition and the RW periodicity is numerically confirmed with LQCD simulations [15–20]

\*takahashi@phys.kyushu-u.ac.jp

†kounoh@cc.saga-u.ac.jp

‡yahiro@phys.kyushu-u.ac.jp

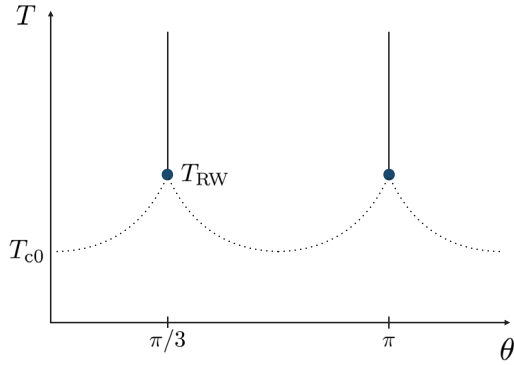


FIG. 1 (color online). QCD phase diagram in the imaginary  $\mu$  region. The solid and dashed lines stand for the RW phase transition and the deconfinement crossover, respectively.

and the underlying mechanism is clearly understood with the effective model [14,21,22] by introducing a new concept of extended  $\mathbb{Z}_{N_c}$  symmetry.

The quark number density  $n_q$  is a fundamental quantity to study high-density physics and important in determining the EOS at finite real  $\mu$ . The EOS plays an essential role in investigating the structure of neutron stars. Moreover,  $n_q$  is useful to determine the strength of vector-type interaction in the effective model [23,24]. For small real  $\mu/T$ , the quark number density was calculated with the Taylor expansion method for the reweighting factor in which either the staggered-type [25] or the Wilson-type quark action [26] is taken. The quark number density is also computed at imaginary  $\mu$  in Refs. [17,18,27–29] with the staggered-type quark action, and  $n_q$  at real  $\mu$  is deduced from that at imaginary  $\mu$  by assuming analytic forms for  $n_q$ .

In this paper, we investigate the  $\mu$  dependence of  $n_q$  at both imaginary and real  $\mu$ . We first perform LQCD simulations at imaginary  $\mu$  with the Wilson-type quark action since the quark number density at imaginary  $\mu$  was not calculated with the Wilson-type quark action. LQCD simulations at imaginary  $\mu$  do not require any special prescription in numerical calculations since there is no sign problem. The  $n_q$  obtained at imaginary  $\mu$  are extrapolated to the real  $\mu$  region by assuming functional forms for  $n_q$ . The extrapolated results are confirmed to be consistent with the previous results [26] of the Taylor expansion method for the reweighting factor. The upper bound  $(\mu/T)_{\max}$  of the region where the extrapolation is considered to be reliable is estimated for each  $T$ .

The hadron resonance gas (HRG) model is reliable in the confinement region. For the  $2+1$ -flavor case at zero chemical potential, in fact, it is shown in Ref. [30] that the model well reproduces LQCD data on pressure at  $T < 1.2T_{c0}$ . As shown by the dashed line in Fig. 1, the pseudocritical temperature  $T_c(\theta)$  of deconfinement transition increases from  $T_{c0}$  to  $T_{RW}$  as  $\theta$  increases from zero to  $\pi/N_c$ . As for real  $\mu$ , meanwhile, the pseudocritical temperature  $T_c(\mu)$  decreases as  $\mu$  increases. When  $\mu$  varies

from the purely imaginary value to the real value with  $T$  fixed at  $T_{c0}$ , the system is, thus, in the confinement phase for imaginary  $\mu$  and in the deconfinement phase for real  $\mu$ . Using this property, one can suggest that  $T$  dependence of nucleon and  $\Delta$ -resonance masses in the vicinity of  $T_{c0}$  can be determined from  $n_q$  at imaginary  $\mu$  by using the HRG model. We test how the suggestion works in this paper.

Actual LQCD simulations are done on an  $8^2 \times 16 \times 4$  lattice with the clover-improved two-flavor Wilson fermion action and the renormalization-group-improved Iwasaki gauge action. We confirmed that the  $n_q$  calculated on an  $8^2 \times 16 \times 4$  lattice are consistent with the previous results [18,29] calculated on a  $16^3 \times 4$  lattice. We then adopted an  $8^2 \times 16 \times 4$  lattice to reduce simulation time and take more trajectories. We consider two temperatures,  $T/T_{c0} = 0.93$  and  $0.99$ , in the confinement region and four temperatures,  $T/T_{c0} = 1.08, 1.20, 1.35,$  and  $2.07$ , in the deconfinement region. Following the previous LQCD simulation [26], we compute  $n_q$  along the line of constant physics at  $m_{PS}/m_V = 0.80$ , where  $m_{PS}$  and  $m_V$  are pseudoscalar- and vector-meson masses, respectively. This corresponds to the case of the pion mass  $m_\pi \sim 616$  MeV and the quark mass  $m_q \sim 130$  MeV [24] for  $T_{c0} \sim 171$  MeV [31]. The analytic continuation is carried out with the Fourier series for  $T < T_{c0}$  and the polynomial series for  $T > T_{RW}$ .

This paper is organized as follows. In Sec. II, we explain the lattice action, the quark number density, and the analytic continuation. In Sec. III, we show our simulation parameters and numerical results for  $n_q$  at both imaginary and real  $\mu$ . In Sec. IV, we test whether  $T$  dependence of nucleon and  $\Delta$ -resonance masses can be determined from LQCD data on  $n_q$  at imaginary  $\mu$  by using the HRG model. Section V is devoted to a summary.

## II. FORMULATION

### A. Lattice action

We use the renormalization-group-improved Iwasaki gauge action  $S_g$  [32] and the clover-improved two-flavor Wilson quark action  $S_q$  [33] defined by

$$S = S_g + S_q, \quad (3)$$

$$S_g = -\beta \sum_x \left( c_0 \sum_{\mu < \nu; \mu, \nu=1}^4 W_{\mu\nu}^{1 \times 1}(x) + c_1 \sum_{\mu \neq \nu; \mu, \nu=1}^4 W_{\mu\nu}^{1 \times 2}(x) \right), \quad (4)$$

$$S_q = \sum_{f=u,d} \sum_{x,y} \bar{\psi}_x^f M_{x,y} \psi_y^f, \quad (5)$$

where  $\beta = 6/g^2$  for the gauge coupling  $g$ ,  $c_1 = -0.331$ ,  $c_0 = 1 - 8c_1$ , and

$$\begin{aligned}
 M_{x,y} = & \delta_{xy} - \kappa \sum_{i=1}^3 \{ (1 - \gamma_i) U_{x,i} \delta_{x+\hat{i},y} + (1 + \gamma_i) U_{y,i}^\dagger \delta_{x,y+\hat{i}} \} \\
 & - \kappa \{ e^{\hat{\mu}} (1 - \gamma_4) U_{x,4} \delta_{x+\hat{4},y} + e^{-\hat{\mu}} (1 + \gamma_4) U_{y,4}^\dagger \delta_{x,y+\hat{4}} \} \\
 & - \delta_{xy} c_{\text{SW}} \kappa \sum_{\mu < \nu} \sigma_{\mu\nu} F_{\mu\nu}. \quad (6)
 \end{aligned}$$

Here  $\kappa$  is the hopping parameter,  $\hat{\mu}$  is the quark chemical potential in lattice units, and the lattice field strength  $F_{\mu\nu}$  is defined as  $F_{\mu\nu} = (f_{\mu\nu} - f_{\mu\nu}^\dagger)/(8i)$  with  $f_{\mu\nu}$  the standard clover-shaped combination of gauge links. For the clover coefficient  $c_{\text{SW}}$ , we take the mean-field value estimated from  $W^{1 \times 1}$  in the one-loop level:  $c_{\text{SW}} = (W^{1 \times 1})^{-3/4} = (1 - 0.8412\beta^{-1})^{-3/4}$  [32]. The value of  $\kappa$  is determined at  $\mu = 0$  for each  $\beta$  along the line of constant physics with  $m_{\text{PS}}/m_V = 0.80$  [31,34,35].

### B. Quark number density

The quark number density  $n_q$  is defined as

$$\frac{n_q}{T^3} = \frac{1}{VT^2} \frac{\partial}{\partial \mu} \ln Z \quad (7)$$

$$= \frac{N_f N_t^3}{N_V} \text{tr} \left[ M^{-1} \frac{\partial M}{\partial \hat{\mu}} \right], \quad (8)$$

where  $V$  is the volume,  $N_f$  is the number of flavors,  $N_t$  is the temporal lattice size,  $N_V$  is the lattice volume, and  $M$  is the fermion matrix. We apply the random-noise method for the trace in Eq. (8). The number of noise vectors is about 4,000. The partition function  $Z$  is  $\mu$  even ( $\mathcal{C}$  even), so that  $n_q$  is  $\mu$  odd ( $\mathcal{C}$  odd) from Eq. (7). This means that  $n_q$  is purely imaginary for imaginary  $\mu$ ; actually,

$$n_q^* = \left( \frac{1}{V} \frac{\partial \ln Z}{\partial (i\theta)} \right)^* = \frac{1}{V} \frac{\partial \ln Z}{\partial (-i\theta)} = -n_q. \quad (9)$$

We have confirmed in our LQCD simulations that the real part of  $n_q$  is zero at imaginary  $\mu$ . For later convenience, we represent the imaginary part of  $n_q$  by  $n_q^1$ :  $n_q^1 = \text{Im}(n_q)$ .

### C. Analytic continuation

Our final interest is  $n_q$  at real  $\mu$ . We then extrapolate the  $n_q$  calculated at imaginary  $\mu$  with LQCD to the real  $\mu$  region, assuming some functional forms for  $n_q$ . As for the pseudocritical line, it is shown in Refs. [20,36–38] that the terms of order higher than  $\mu^2$  are necessary.

In the imaginary- $\mu$  region,  $n_q$  is a  $\theta$ -odd function with the RW periodicity. We then consider only a period  $-\pi/3 < \theta \leq \pi/3$  for simplicity. In the confinement region at  $T < T_{c0}$ , the quark number density is smooth for any  $\theta$ , indicating that  $n_q = 0$  at  $\theta = 0, \pm\pi/3$  [14,21,22]. Hence  $n_q$  can be described with good accuracy by a partial sum  $S_F^n(T, \theta)$  of the Fourier series,

$$\frac{n_q(T, i\theta)}{T^3} \approx i S_F^n(T, \theta) = i \sum_{k=1}^n a_F^{(k)}(T) \sin(3k\theta), \quad (10)$$

where the superscript  $n$  of  $S_F^n(T, \theta)$  represents the highest order in the partial sum. The coefficients  $a_F^{(k)}(T)$  are obtained by fitting the function (10) to LQCD data at imaginary  $\mu = i\mu_I$ . The analytic continuation from  $\mu = i\mu_I$  to  $\mu = \mu_R$  can be made by replacing  $i\mu_I/T$  with  $\mu_R/T$  in Eq. (10):

$$\begin{aligned}
 \frac{n_q(T, \mu_R/T)}{T^3} & \approx g_F^n \left( T, \frac{\mu_R}{T} \right) \\
 & = \sum_{k=1}^n a_F^{(k)}(T) \sinh \left( 3k \frac{\mu_R}{T} \right). \quad (11)
 \end{aligned}$$

Here note that the coefficients  $a_F^{(k)}(T)$  have already been determined at imaginary  $\mu$ .

In the region  $T_{c0} < T < T_{\text{RW}}$ , the system is in the deconfinement region for small  $\theta$  but in the confinement region for large  $\theta$  near  $\pi/3$ , as shown in Fig. 1. Because of this property, the  $\theta$  dependence of  $n_q$  is complicated and makes the analytic continuation difficult. We then do not perform the analytic continuation in this region.

In the deconfinement region at  $T > T_{\text{RW}}$ , the quark number density is discontinuous at  $\theta = \pm\pi/3$  where the first-order RW phase transition takes place; note that  $n_q$  is the order parameter of the RW first-order transition [14]. Owing to this property,  $n_q$  monotonically increases with  $\theta$ , as shown later in Fig. 2. This suggests that  $n_q$  can be described with good accuracy by a partial sum  $S_p^{2n-1}(T, \theta)$  of the polynomial series,

$$\frac{n_q(T, i\theta)}{T^3} \approx i S_p^{2n-1}(T, \theta) = i \sum_{k=1}^n a_p^{(2k-1)}(T) \theta^{2k-1}, \quad (12)$$

where the superscript  $n$  of  $S_p^{2n-1}(T, \theta)$  represents the highest order in the partial sum. Again, the analytic

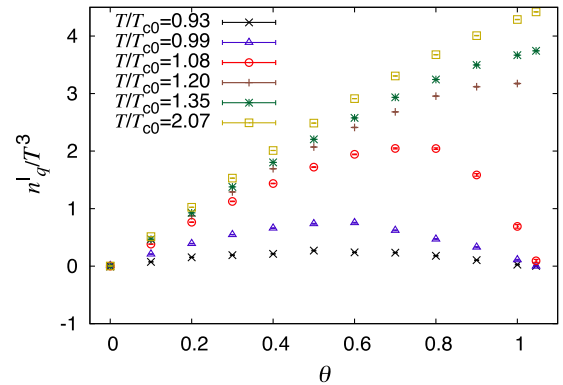


FIG. 2 (color online).  $\mu_1/T$  dependence of  $n_q^1/T^3$  at various values of  $T$ . The LQCD data are shown by symbols with error bars, although the error bars are quite small.

continuation is made by replacing  $i\mu_1/T$  with  $\mu_R/T$  in Eq. (12):

$$\begin{aligned} \frac{n_q(T, \mu_R/T)}{T^3} &\approx g_p^{2n-1} \left( T, \frac{\mu_R}{T} \right) \\ &= \sum_{k=1}^n (-1)^{(k-1)} a_p^{(2k-1)}(T) \left( \frac{\mu_R}{T} \right)^{2k-1}. \end{aligned} \quad (13)$$

### III. NUMERICAL RESULTS

Full QCD configurations with  $N_f = 2$  dynamical quarks were generated with the hybrid Monte Carlo algorithm on a lattice of  $N_x \times N_y \times N_z \times N_t = 8^2 \times 16 \times 4$ . The step size of the molecular dynamics is  $\delta\tau = 0.02$  and the step number is  $N_\tau = 50$ . The acceptance ratio is more than 95%. We generated about 32,000 trajectories and removed the first 4,000 trajectories for the thermalization of all the parameters and measured  $n_q$  at every 100 trajectories. The relation of parameters  $\kappa$  and  $\beta$  to the corresponding  $T/T_{c0}$  was determined in Refs. [31,34,35]; see Table I for the relation.

#### A. Quark number density at imaginary $\mu$

Figure 2 shows  $n_q^1/T^3$  as a function of  $\theta$  for all the temperatures we consider. The LQCD data are plotted by symbols with error bars, although the errors are quite small. The number density  $n_q^1$  should be zero at  $\theta = \pi/3$  below  $T_{RW}$  but finite above  $T_{RW}$ , since  $n_q^1$  is the order parameter of the first-order RW phase transition. One can see from this fact that  $T_{RW}$  is located between  $1.08$  and  $1.2T_{c0}$ . The quark number density  $n_q^1/T^3$  behaves as the sine function for  $T < T_{c0}$ , but monotonically increases up to  $\theta = \pi/3$  for  $T > T_{RW}$ . As for  $T = 1.08T_{c0}$ , the system is in the deconfinement region for  $\theta < 0.8$  but in the confinement region for  $0.8 < \theta < \pi/3$ , since  $n_q^1/T^3$  increases monotonically up to  $\theta \sim 0.7$  but decreases to zero for  $\theta > 0.8$ . This result is consistent with that of the staggered-type fermion in Ref. [29]. The present result is, thus, independent of the fermion action taken.

TABLE I. Summary of the simulation parameter sets determined in Refs. [31,34,35]. Note that  $T_{c0} \approx 171$  MeV, where  $T_{c0}$  is the pseudocritical temperature of deconfinement transition at  $\mu = 0$ . In the parameter setting, the lattice spacing  $a$  is about  $0.14$ – $0.2$  fm.

$\kappa$	$\beta$	$T/T_{c0}$
0.141139	1.80	0.93(5)
0.140070	1.85	0.99(5)
0.138817	1.90	1.08(5)
0.137716	1.95	1.20(6)
0.136931	2.00	1.35(7)
0.135010	2.20	2.07(10)

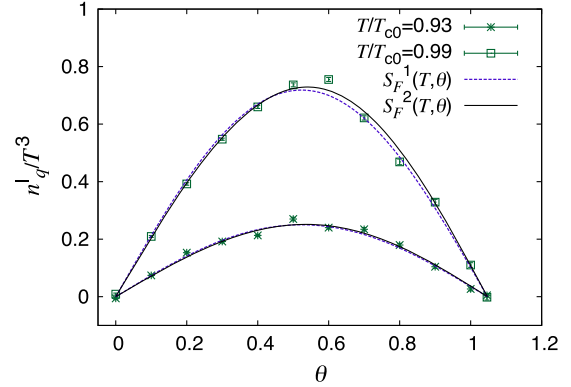


FIG. 3 (color online). Results of  $\chi^2$  fitting to LQCD data for the case of  $T < T_{c0}$ . The results of  $S_F^1$  and  $S_F^2$  are plotted by dashed and solid lines, respectively. LQCD data are shown by symbols with error bars.

First we consider the case of  $T < T_{c0}$  and determine the coefficients  $a_F^{(k)}(T)$  of the Fourier series from the  $n_q$  calculated at imaginary  $\mu$  with LQCD. In principle,  $n_q$  is described as an infinite series of sine functions for imaginary  $\mu$  and of hyperbolic sine functions for real  $\mu$ , as shown in Eqs. (10) and (11). The partial sum is valid only when the series converges. Particularly for real  $\mu$ , the hyperbolic sine functions increase rapidly as  $\mu/T$  becomes large. In this sense, it is important that the coefficients  $a_F^{(k)}$  become small rapidly as  $k$  increases.

In Fig. 3, the results of  $\chi^2$  fitting are compared with the LQCD results. Here, two cases of  $S_F^1$  and  $S_F^2$  are plotted by dashed and solid curves, respectively. The two results well reproduce the LQCD data.

The coefficients obtained are tabulated in Table II for three cases of  $S_F^1$ ,  $S_F^2$ , and  $S_F^3$  and two cases of  $T = 0.93T_{c0}$  and  $0.99T_{c0}$ , together with the values of  $\chi^2$  per degree of freedom (dof). As for  $T = 0.93T_{c0}$ , the absolute value of  $a_F^{(2)}$  is much smaller than  $a_F^{(1)}$  in  $S_F^2$ , but  $a_F^{(3)}$  is comparable to the absolute value of  $a_F^{(2)}$  in  $S_F^3$ . In addition, the  $\chi^2/\text{dof}$  value little changes between  $S_F^2$  and  $S_F^3$ . The result of  $S_F^2$  is, thus, acceptable, but that of  $S_F^3$  is not. Similar discussion is possible for  $T = 0.99T_{c0}$ ; note that the absolute value of  $a_F^{(2)}$  is comparable to that of  $a_F^{(3)}$  in  $S_F^3$  if the error ranges of  $a_F^{(2)}$  and  $a_F^{(3)}$  are taken into account. As shown in Fig. 3, moreover, the deviation of LQCD data from the solid line (the result of  $S_F^2$ ) is rapidly oscillating with  $\theta$  and cannot be reproduced by the next-order term  $\sin(9\theta)$ . Thus, the coefficients higher than  $a_F^{(2)}$  may not be determined from the present LQCD data. We then consider  $S_F^1$  and  $S_F^2$  as the extrapolation function from imaginary  $\mu$  to real  $\mu$ .

Next we consider the case of  $T > T_{RW}$  and determine the coefficients  $a_p^{(2k-1)}(T)$  of the polynomial series. In Fig. 4, the fitting results are compared with LQCD data for  $S_p^3$  in



TABLE II. Coefficients of the Fourier series for  $S_F^1$ ,  $S_F^2$ , and  $S_F^3$ .

$T/T_{c0}$	$a_F^{(1)}$	$a_F^{(2)}$	$a_F^{(3)}$	$\chi^2/\text{dof}$	$\mu_1/T$ (fitting range)
0.93	0.250(2)			5.937	$0 \sim \pi/3$
0.93	0.251(2)	-0.00457(216)		6.084	$0 \sim \pi/3$
0.93	0.251(2)	-0.00526(219)	0.00440(214)	6.290	$0 \sim \pi/3$
0.99	0.718(2)			11.06	$0 \sim \pi/3$
0.99	0.728(3)	-0.0179(26)		7.453	$0 \sim \pi/3$
0.99	0.727(3)	-0.0137(30)	-0.00825(276)	7.288	$0 \sim \pi/3$

panel (a) and for  $S_p^5$  in panel (b). For each case of  $T = 1.20T_{c0}$ ,  $1.35T_{c0}$ , and  $2.07T_{c0}$ , two dashed lines stand for the upper and lower bounds of  $\chi^2$  fitting, respectively. The fitting results well reproduce LQCD data. The resulting coefficients  $a_p^{(2k-1)}(T)$  are tabulated in Table III for three cases of  $S_p^3$ ,  $S_p^5$ , and  $S_p^7$ , together with the  $\chi^2/\text{dof}$  values. For each temperature,  $S_p^7$  has the smallest  $\chi^2/\text{dof}$  value among  $S_p^3$ ,  $S_p^5$ , and  $S_p^7$ . Particularly at  $T = 1.35T_{c0}$ , the value is almost one. Nevertheless, for each temperature the absolute value of  $a_p^{(7)}$  is comparable to that of  $a_p^{(5)}$  in  $S_p^7$ , whereas the absolute value of  $a_p^{(5)}$  is smaller than that of  $a_p^{(3)}$  in  $S_p^5$  by about an order of magnitude. We also performed a fit with ratios of polynomials to take account of the terms of order higher than  $a_p^{(7)}$ , following Ref. [37]. The resulting  $\chi^2/\text{dof}$  value is much larger than the case of  $S_p^7$ . This may indicate that  $a_p^{(7)}$  and its higher-order coefficients cannot be determined properly from the present LQCD data. We then use  $S_p^3$  and  $S_p^5$  as the extrapolation function from imaginary  $\mu$  to real  $\mu$ .

### B. Quark number density at real $\mu$

First we consider the case of  $T/T_{c0} < 1$ . As the extrapolation function from imaginary  $\mu$  to real  $\mu$ , we consider  $g_F^1$  and  $g_F^2$ . Figure 5 shows the  $\mu/T$  dependence of  $n_q/T^3$  for  $T = 0.99T_{c0}$ . The result of the extrapolation is

shown by a pair of lines; the two lines correspond to the upper and lower bounds of the extrapolation and the uncertainty comes from the errors in  $a_F^{(k)}$ . The  $g_F^2$  case (solid line) has a larger error than the  $g_F^1$  case (dashed line), because the former error comes from both  $a_F^{(1)}$  and  $a_F^{(2)}$  but the latter comes only from  $a_F^{(1)}$ . We also use symbols with error bars to show the previous LQCD result [26] of the Taylor expansion method for the reweighting factor. In the previous calculation,  $n_q$  is described by a polynomial series of  $\mu/T$  and the terms up to  $(\mu/T)^3$  are taken into account. The result of  $g_F^2$  deviates from that of the Taylor expansion method at  $\mu/T > 0.8$ . To clarify what causes the deviation, in Eq. (11) for  $g_F^2$ , we expand the hyperbolic sine function into a polynomial series and discard the terms of order higher than  $(\mu/T)^3$ . We denote the resulting function by  $\bar{g}_F^2$ . The result of  $\bar{g}_F^2$  (dotted line) is consistent with that of the Taylor expansion method at  $\mu/T < 1$ . Thus, the difference between  $g_F^2$  and the Taylor expansion method comes from the terms of order higher than  $(\mu/T)^3$ , and  $g_F^2$  yields a correction to the result of the Taylor expansion. From the fact that the correction is small at  $\mu/T < 0.8$ , we can conclude that both the previous result of the Taylor expansion method and the present result of  $g_F^2$  are reliable at least at  $\mu/T < 0.8$ .

Figure 6 shows  $\mu/T$  dependence of  $n_q/T^3$  at  $T = 0.93T_{c0}$ . The definition of lines is the same as in Fig. 5. The difference between the two results of  $g_F^1$  and  $g_F^2$

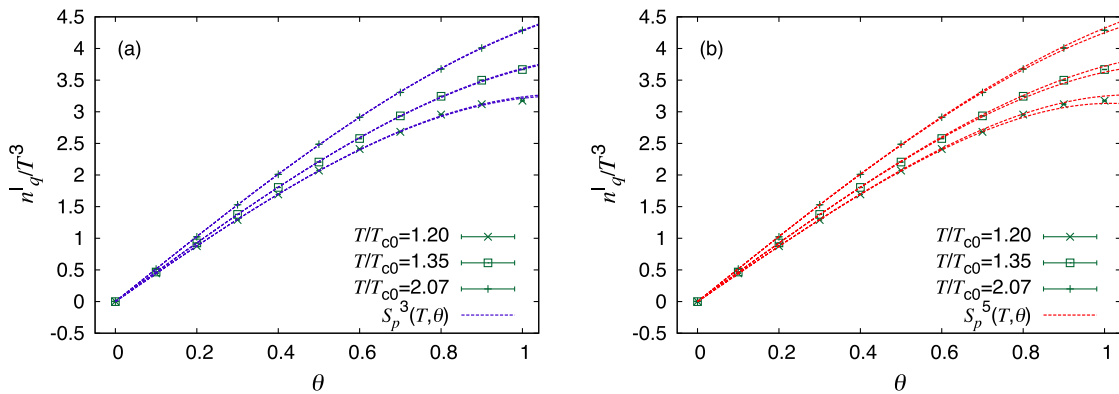


FIG. 4 (color online). Results of  $\chi^2$  fitting to LQCD data for the case of  $T > T_{RW}$ . Panels (a) and (b) show the results of  $S_p^3$  and  $S_p^5$ , respectively. For each temperature, two dashed lines correspond to the upper and lower bounds of the  $\chi^2$  fitting, respectively. LQCD data are shown by symbols with error bars.

TABLE III. Coefficients of the polynomial series for  $S_p^3$ ,  $S_p^5$ , and  $S_p^7$ .

$T/T_{c0}$	$a_p^{(1)}$	$a_p^{(3)}$	$a_p^{(5)}$	$a_p^{(7)}$	$\chi^2/\text{dof}$	$\mu_1/T$ (fitting range)
1.20	4.437(4)	-1.214(7)			13.66	0-1
1.20	4.407(5)	-1.024(27)	-0.1935(260)		8.472	0-1
1.20	4.427(7)	-1.274(66)	-0.4458(1569)	-0.4229(1024)	7.245	0-1
1.35	4.675(3)	-0.9973(49)			6.036	0-1
1.35	4.662(5)	-0.9223(223)	-0.06736(1956)		5.308	0-1
1.35	4.695(7)	-1.295(67)	-0.7986(1469)	-0.5310(893)	1.011	0-1
2.07	5.174(2)	-0.8904(40)			9.161	0-1
2.07	5.177(4)	-0.9056(177)	0.01356(1531)		10.21	0-1
2.07	5.158(6)	-0.7119(432)	0.4381(932)	0.2819(574)	8.220	0-1

reduces as  $T$  decreases from  $0.99$  to  $0.93T_{c0}$ . The extrapolation of  $g_F^2$ , thus, becomes more reliable as  $T$  decreases. As mentioned above, the  $g_F^2$  extrapolation is reliable at least at  $\mu/T < 0.8$  for  $T = 0.99T_{c0}$ . This means that for

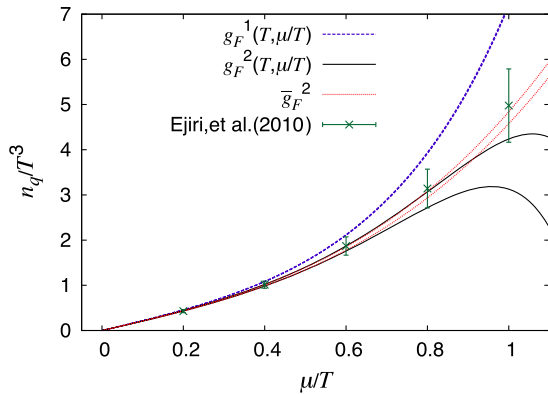


FIG. 5 (color online).  $\mu/T$  dependence of  $n_q/T^3$  at  $T = 0.99T_{c0}$ . The results of  $g_F^1$ ,  $g_F^2$ , and  $\bar{g}_F^2$  are plotted by dashed, solid, and dotted lines, respectively; see the text for the definition of  $\bar{g}_F^2$ . For each case, the upper and lower bounds of  $\chi^2$  fittings are shown by a pair of lines. The symbols denote LQCD results of the Taylor expansion method for the reweighting factor in Ref. [26].

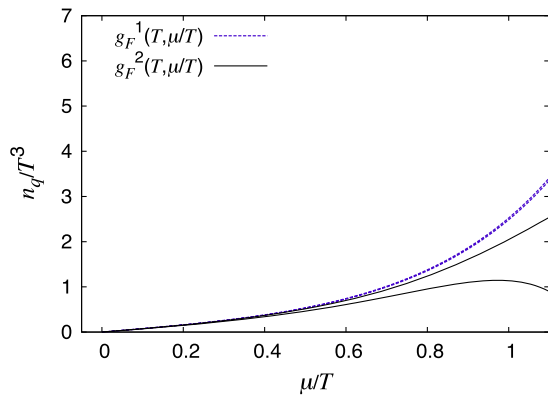


FIG. 6 (color online).  $\mu/T$  dependence of  $n_q/T^3$  at  $T = 0.93T_{c0}$ . See Fig. 5 for the definition of lines. Two cases of  $g_F^1$  and  $g_F^2$  are plotted.

$T = 0.93T_{c0}$  as well, the  $g_F^2$  extrapolation is reliable at least at  $\mu/T < 0.8$ .

Next we consider the case of  $T > T_{RW}$ . As the extrapolation function from imaginary  $\mu$  to real  $\mu$ , we consider  $g_p^3$  and  $g_p^5$ . Figures 7, 8, and 9 show the  $\mu/T$  dependence of  $n_q/T^3$  at  $T = 1.20T_{c0}$ ,  $1.35T_{c0}$ , and  $2.07T_{c0}$ , respectively. The result of  $g_p^3$  ( $g_p^5$ ) is plotted by a pair of dashed (solid) lines; the two lines correspond to the upper and lower bounds of extrapolation. For each temperature, the result of  $g_p^3$  agrees with the previous result [26] of the Taylor expansion method for the reweighting factor. In the Taylor expansion method,  $n_q$  is described by a polynomial series and the terms up to  $(\mu/T)^3$  are taken. The highest order taken is the same in the  $g_p^3$  extrapolation and the Taylor expansion method. Thus, the agreement of  $n_q$  between the two methods is natural, although the coefficients are determined with different procedures in the two methods. The difference between  $g_p^3$  and  $g_p^5$  becomes small as  $T$  increases. Contributions of order higher than  $(\mu/T)^3$ , thus, become small as  $T$  increases.

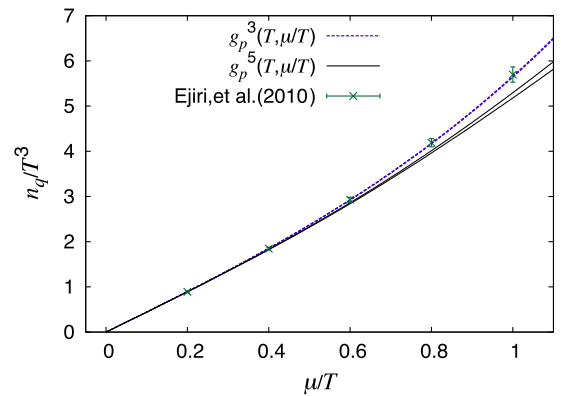


FIG. 7 (color online).  $\mu/T$  dependence of  $n_q/T^3$  at  $T = 1.20T_{c0}$ . Two cases of  $g_p^3$  and  $g_p^5$  are plotted. The upper and the lower bounds of  $\chi^2$  fitting are shown by a pair of dashed lines for  $g_p^3$  and by a pair of solid lines for  $g_p^5$ . The symbols denote LQCD results of the Taylor expansion method for the reweighting factor in Ref. [26].

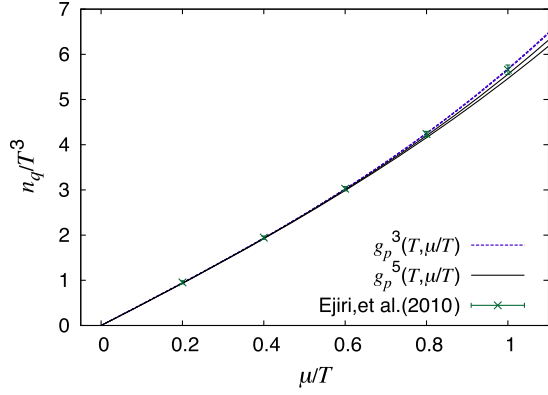


FIG. 8 (color online).  $\mu/T$  dependence of  $n_q/T^3$  at  $T = 1.35T_{c0}$ . Two cases of  $g_p^3$  and  $g_p^5$  are plotted. See Fig. 7 for the definition of lines. The symbols denote LQCD results of the Taylor expansion method for the reweighting factor in Ref. [26].

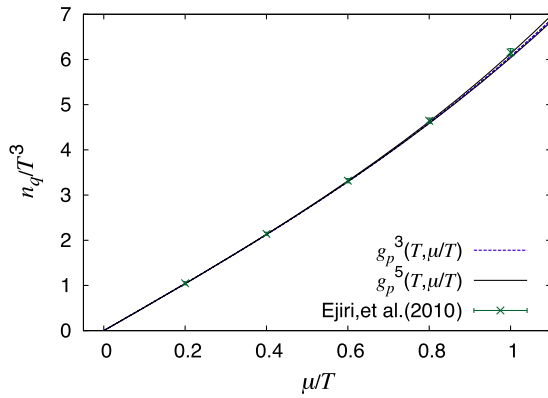


FIG. 9 (color online).  $\mu/T$  dependence of  $n_q/T^3$  at  $T = 2.07T_{c0}$ . Two cases of  $g_p^3$  and  $g_p^5$  are plotted. See Fig. 7 for the definition of lines. The symbols denote LQCD results of the Taylor expansion method for the reweighting factor in Ref. [26].

Now we estimate the upper bound  $(\mu/T)_{\max}$  of the region in which the extrapolation is considered to be reliable and investigate  $T$  dependence of  $(\mu/T)_{\max}$  for  $T > T_{RW}$ . For this purpose, we define the relative difference  $\delta$  between  $g_p^3$  and  $g_p^5$  as  $\delta = |g_p^5 - g_p^3|/g_p^5$  and assume that the extrapolation is reliable when  $\delta < 0.1$ . The relative difference  $\delta$  exceeds 10% at  $\mu/T \approx 0.72$  for  $T = 1.20T_{c0}$ ,  $\mu/T \approx 1.2$  for  $T = 1.35T_{c0}$  and  $\mu/T \approx 2.6$  for  $T = 2.07T_{c0}$ , as shown in Fig. 10. The upper bound  $(\mu/T)_{\max}$  of the reliable extrapolation is plotted as a function of  $T/T_{c0}$  in Fig. 11. The upper bound goes up as  $T$  increases, indicating that contributions of order higher than  $(\mu/T)^3$  become less important as  $T$  becomes high. Thus, the present result of  $g_p^3$  and the previous result [26] of the Taylor expansion method become more reliable as  $T$  increases.

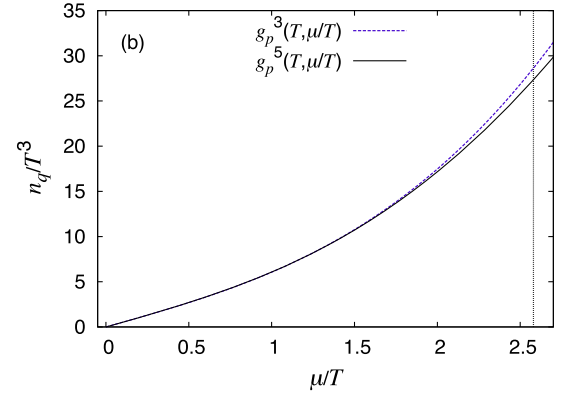
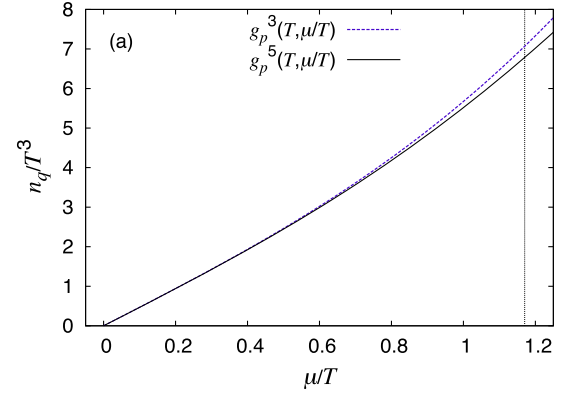


FIG. 10 (color online).  $\mu/T$  dependence of  $n_q/T^3$  and the region of  $\delta \leq 0.1$  for (a)  $T = 1.35T_{c0}$  and (b)  $T = 2.07T_{c0}$ . The relative difference  $\delta$  exceeds 10% at  $\mu/T = (\mu/T)_{\max}$  represented by the vertical dotted line. The dashed and solid lines denote the mean values of  $g_p^3$  and  $g_p^5$ , respectively.

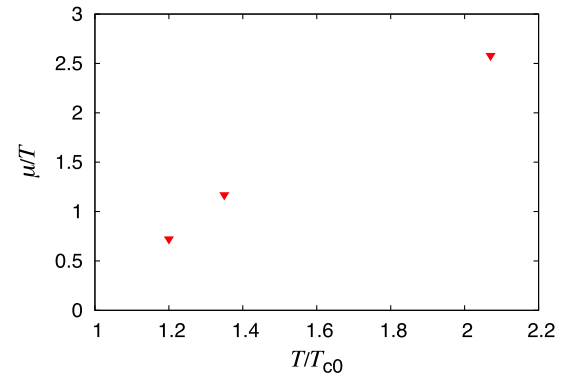


FIG. 11 (color online).  $T$  dependence of the upper bound  $(\mu/T)_{\max}$  of the reliable extrapolation for the case of  $T > T_{RW}$ .

#### IV. HADRON RESONANCE GAS MODEL

Now we consider the confinement region at  $\theta \geq 0$  and test whether nucleon and  $\Delta$ -resonance masses can be determined from the present LQCD results at  $\theta \geq 0$  by using the HRG model particularly in the vicinity of  $T_{c0}$ . The HRG model considers noninteracting hadrons and

resonances, each classified with species  $i$ , i.e., with mass  $m_i$ , baryon number  $B_i$  and isospin  $I_{3i}$ . For the 2 + 1-flavor case at zero chemical potential, the HRG model well reproduces LQCD data on pressure at  $T < 1.2T_{c0}$  [30]. This means that the HRG model is applicable at  $T < T_{c0}$  even if  $\theta$  is finite, because  $T_c(\theta) > T_{c0}$  for any finite  $\theta$ . The pressure of the model is obtained by

$$p^{\text{HRG}} = -\frac{T}{V} \sum_{i \in \text{meson}} \ln Z_i^{\text{M}}(T, V, \mu_i) - \frac{T}{V} \sum_{i \in \text{baryon}} \ln Z_i^{\text{B}}(T, V, \mu_i) \quad (14)$$

with

$$\ln Z_i^{\text{M/B}} = \pm \frac{V g_i}{2\pi^2} \int_0^\infty dp p^2 \ln(1 \mp z_i e^{-\epsilon_i/T}) \quad (15)$$

for the energy  $\epsilon_i = \sqrt{p^2 + m_i}$ , the degeneracy factor  $g_i$ , and the fugacity

$$z_i = e^{\mu_i/T} = \exp\left(\frac{B_i \mu_B + 2I_{3i} \mu_{\text{iso}}}{T}\right), \quad (16)$$

where  $\mu_B (\equiv 3\mu)$  and  $\mu_{\text{iso}}$  are the baryon and isospin chemical potentials, respectively. Here we consider only the case of  $\mu_{\text{iso}} = 0$ . The baryon number density is easily obtained as

$$n_B^{\text{HRG}} = -\frac{\partial}{\partial \mu_B} p^{\text{HRG}}. \quad (17)$$

There are lattice artifacts in LQCD simulations. These were already discussed in Refs. [25,26,39–41]. For small  $N_t$ , for example, thermodynamic quantities exceed the Stefan-Boltzmann (SB) limit. Since it is not easy to eliminate the lattice artifact exactly, we take the following simple

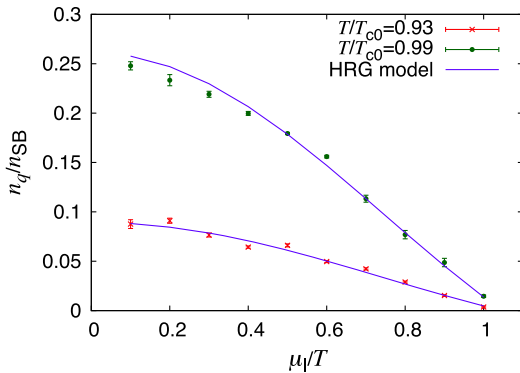


FIG. 12 (color online).  $\theta$  dependence of  $n_q/n_{\text{SB}}$  at  $T = 0.93$  and  $0.99T_{c0}$ . The cross and square symbols with error bars represent the LQCD results at  $T = 0.93$  and  $0.99T_{c0}$ , respectively, whereas the solid lines stand for the HRG model results.

TABLE IV. Results of  $\chi^2$  fitting for baryon masses  $m_N$  and  $m_\Delta$  in the HRG model and  $\chi^2/\text{dof}$  values.

$T/T_{c0}$	$m_N(\text{MeV})$	$m_\Delta(\text{MeV})$	$\chi^2/\text{dof}$
0.93	1091	1547	6.625
0.99	940	1385	7.993

prescription. We consider the lattice SB limit that is defined by the lattice action with massless and free quarks and normalize LQCD results with the corresponding values in the lattice SB limit in order to reduce the lattice artifacts; see Appendix A for the quark number density in the lattice SB limit. For the HRG model, meanwhile, the quark number density is normalized by the value in the continuum SB limit. In the HRG model, we assume that nucleon mass  $m_N$  and  $\Delta$ -resonance mass  $m_\Delta$  depend only on  $T$ . The baryon masses are determined so as to reproduce the LQCD result. Here we assume that the masses of 24 resonance states above the mass threshold  $m_{\text{cut}}^B$  are fixed at 1.8 GeV, following Ref. [39]. But the contribution of 24 states to  $n_q$  is small.

Figure 12 shows the  $\theta$  dependence of the normalized quark number density  $n_q/n_{\text{SB}}$  for  $T = 0.93$  and  $0.99T_{c0}$ . The HRG-model results (solid lines) well reproduce the  $\theta$  dependence of LQCD results (symbols with error bars) for both cases,  $T = 0.93$  and  $0.99T_{c0}$ . This implies that  $m_N$  and  $m_\Delta$  depend little on  $\theta$ . The resulting nucleon and  $\Delta$ -resonance masses are shown in Table IV, together with  $\chi^2/\text{dof}$  values. The  $\chi^2/\text{dof}$  values are close to those for  $g_F^2$  in Table II. The resulting masses are heavier than the corresponding physical values because the quark mass is much heavier than the physical value in our simulations. As shown in Table IV, both  $m_N$  and  $m_\Delta$  decrease by about 10% as  $T$  increases from 0.93 to  $0.99T_{c0}$ .

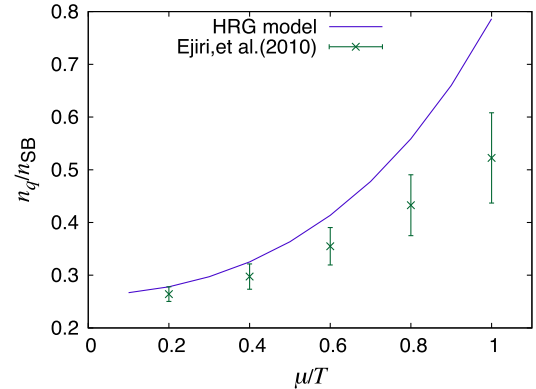


FIG. 13 (color online).  $\mu/T$  dependence of  $n_q/n_{\text{SB}}$  in the real  $\mu$  region for  $T = 0.99T_{c0}$ . The symbols with error bars stand for LQCD results of the Taylor expansion method for the reweighting factor in Ref. [26], while the solid line is the result of the HRG model.



Finally we consider the case of real  $\mu$ . The HRG model becomes less reliable as  $\mu$  increases, because the pseudocritical temperature  $T_c(\mu)$  of deconfinement transition goes down from  $T_{c0}$  as  $\mu$  increases from zero. Figure 13 shows the  $\mu/T$  dependence of  $n_q/n_{SB}$  at  $T = 0.99T_{c0}$ . In the range  $\mu/T < 0.4$ , the HRG model result (solid line) is consistent with the previous LQCD results [26] (symbols with error bars) based on the Taylor expansion method for the reweighting factor. Beyond the range, the HRG model overestimates the LQCD results. The HRG model is, thus, reliable only at  $\mu/T < 0.4$  for the case of  $T = 0.99T_{c0}$ .

## V. SUMMARY

We have investigated  $\mu$  dependence of  $n_q$  at imaginary and real  $\mu$ , performing LQCD simulations at imaginary  $\mu$  and extrapolating the results to the real- $\mu$  region by assuming functional forms for  $n_q$ . LQCD calculations were done on an  $8^2 \times 16 \times 4$  lattice with the clover-improved two-flavor Wilson fermion action and the renormalization-group-improved Iwasaki gauge action. We considered two temperatures below  $T_{c0}$  and four temperatures above  $T_{c0}$ . The quark number density was computed along the line of constant physics at  $m_{PS}/m_V = 0.80$ .

For imaginary  $\mu$ , the quark number density calculated with the Wilson-type fermion action is consistent with the previous result [29] based on the staggered-type fermion action. The LQCD results, thus, do not depend on the fermion action taken.

We have extrapolated  $n_q$  at imaginary  $\mu$  to real  $\mu$ , assuming the Fourier series  $g_F^n$  for  $T < T_{c0}$  and the polynomial series  $g_p^{2n-1}$  for  $T > T_{RW}$ ; here the superscript  $n$  represents the highest order in the partial sum. As for  $T = 0.99T_{c0}$ , the present result of  $g_F^2$  is consistent with the previous result [26] of the Taylor expansion method for the reweighting factor in the range  $\mu/T < 0.8$ . The extrapolation based on  $g_F^2$  is, thus, reliable at  $\mu/T < 0.8$  for  $T = 0.99T_{c0}$ . Furthermore, the difference between the two results of  $g_F^1$  and  $g_F^2$  reduces as  $T$  decreases from  $T_{c0}$ , indicating that higher-order contributions become less important as  $T$  decreases. Therefore, the extrapolation based on  $g_F^2$  is reliable at  $\mu/T < 0.8$  for any  $T$  less than  $T_{c0}$ .

For  $T > T_{RW}$ , the previous study based on the Taylor expansion method for the reweighting factor has contributions up to  $(\mu/T)^3$ , but the present  $g_p^5$  extrapolation retains contributions up to  $(\mu/T)^5$ . Using this advantage of the present method from the previous method, we have estimated to what extent the Taylor expansion or the  $g_p^3$  extrapolation works. The upper bound  $(\mu/T)_{\max}$  of the reliable extrapolation goes up as  $T$  increases from  $T_{RW}$ , because higher-order contributions become less important.

The HRG model is reliable in the confinement region. For the  $2 + 1$ -flavor case at zero chemical potential, in fact, the HRG model well reproduces LQCD data on pressure at

$T < 1.2T_{c0}$ [30]. When  $\mu$  is varied with  $T$  fixed at  $T_{c0}$ , the system is in the confinement phase at imaginary  $\mu$  but in the deconfinement phase at real  $\mu$ . This means that the HRG model is more reliable at imaginary  $\mu$  than at real  $\mu$ , when  $T$  is fixed at  $T_{c0}$ . We have then tested whether  $T$  dependence of  $m_N$  and  $m_\Delta$  in the vicinity of  $T_{c0}$  can be determined from LQCD data on  $n_q$  at imaginary  $\mu$  by using the HRG model. The HRG model well reproduces the LQCD results, when  $m_N$  and  $m_\Delta$  are assumed to depend on  $T$  only. This implies that  $m_N$  and  $m_\Delta$  little depend on  $\theta(= \mu_1/T)$ . In our test calculation,  $m_N$  and  $m_\Delta$  reduce by about 10% when  $T$  increases from  $0.93T_{c0}$  to  $0.99T_{c0}$ . We propose this method as a handy way of determining  $T$  dependence of  $m_N$  and  $m_\Delta$  in the vicinity of  $T_{c0}$ . This method is practical, since it is not easy to measure  $T$  dependence of pole masses directly with LQCD simulations.

## ACKNOWLEDGMENTS

We thank A. Nakamura and K. Nagata for useful discussions and giving the LQCD program codes. We are also grateful to I.-O. Stamatescu, T. Sasaki and T. Saito for helpful discussions. J. T., H. K., and M. Y. are supported by Grant-in-Aid for Scientific Research (No. 25-3944, No. 26400279 and No. 26400278) from the Japan Society for the Promotion of Science (JSPS). The numerical calculations were performed on NEC SX-9 and SX-8R at CMC, Osaka University and on HITACHI HA8000 at Research Institute for Information Technology, Kyushu University.

## APPENDIX: QUARK NUMBER DENSITY FOR THE WILSON FERMION IN THE MASSLESS FREE-GAS LIMIT

We consider  $n_q$  for the Wilson fermion in the lattice SB limit (the massless free-gas limit). In the high- $T$  limit, we can consider a quark as a massless and noninteracting particle, since the effects of finite quark mass and interactions between quarks are negligible there. In the Appendix of Ref. [26], the lattice SB limit is discussed except for the quark number density.

The partition function with free Wilson fermions is given by

$$Z(\kappa, \hat{\mu}) = (\det M)^{N_f}, \quad (\text{A1})$$

$$M_{xy} = \delta_{xy} - \kappa \sum_{i=1}^3 [(1 - \gamma_i)\delta_{x+\hat{i},y} + (1 + \gamma_i)\delta_{x-\hat{i},y}] - \kappa[e^{+\hat{\mu}}(1 - \gamma_4)\delta_{x+\hat{4},y} + e^{-\hat{\mu}}(1 + \gamma_4)\delta_{x-\hat{4},y}] \quad (\text{A2})$$

on an  $N_x \times N_y \times N_z \times N_t$  lattice. After the unitary transformation to momentum space, we obtain

$$Z(1/8, \hat{\mu}) = \left( \prod_k \det \tilde{M}(k) \right)^{N_c N_f} \quad (\text{A3})$$

for the time component. The quark number density in the lattice SB limit is then obtained as

$$\det \tilde{M}(k) = \frac{16}{8^4} \left[ \sum_i \sin^2 k_i + \left\{ 2 \sum_i \sin^2 \left( \frac{k_i}{2} \right) \right\}^2 + 4 \left\{ 2 \sum_i \sin^2 \left( \frac{k_i}{2} \right) + 1 \right\} \sin^2 \left( \frac{k_t - i\hat{\mu}}{2} \right) \right]^2 \quad (\text{A4})$$

$$\begin{aligned} \frac{n_q}{T^3} &= \frac{N_t^3}{N_V} \frac{\partial}{\partial \hat{\mu}} \ln Z(1/8, \hat{\mu}) \\ &= N_c N_f \frac{N_t^3}{N_V} \sum_k \frac{\partial \det \tilde{M}(k)}{\partial \hat{\mu}} [\det \tilde{M}(k)]^{-1} \end{aligned} \quad (\text{A7})$$

in the massless quark limit  $\kappa = 1/8$ , where  $\tilde{M}$  is the fermion matrix in momentum space, and

$$k_i = \frac{2\pi j_i}{N_i}, \quad j_i = 0, \pm 1, \dots, N_i/2 \quad (\text{A5})$$

with

$$\begin{aligned} \frac{\partial \det \tilde{M}(k)}{\partial \hat{\mu}} &= -\frac{1}{8^2} \left\{ 2 \sum_i \sin^2 \left( \frac{k_i}{2} \right) + 1 \right\} \\ &\times (\sinh \hat{\mu} \cos k_t + i \cosh \hat{\mu} \sin k_t). \end{aligned} \quad (\text{A8})$$

for the spatial components ( $i = x, y, z$ ) and

$$k_t = \frac{2\pi(j_t + 1/2)}{N_t}, \quad j_t = 0, \pm 1, \dots, N_t/2 \quad (\text{A6})$$

The quark number density at imaginary  $\mu$  is obtained by replacing  $\hat{\mu}$  with  $i\hat{\mu}_I$  in Eqs. (A7) and (A8).

- 
- [1] P. B. Demorest, T. Pennucci, S. M. Ransom, M. S. E. Roberts, and J. W. T. Hessels, *Nature (London)* **467**, 1081 (2010).
- [2] L. Kumar (STAR Collaboration), *Nucl. Phys.* **A904–A905**, 256c (2013).
- [3] E. O’Brien (PHENIX Collaboration), *Nucl. Phys.* **A904–A905**, 264c (2013).
- [4] S. Muroya, A. Nakamura, C. Nonaka, and T. Takaishi, *Prog. Theor. Phys.* **110**, 615 (2003).
- [5] P. de Forcrand, *Proc. Sci.*, LAT2009 (2009) 010.
- [6] G. Aarts, *Phys. Rev. Lett.* **102**, 131601 (2009).
- [7] G. Aarts, L. Bongiovanni, E. Seiler, D. Sexty, and I.-O. Stamatescu, *Eur. Phys. J. A* **49**, 89 (2013).
- [8] D. Sexty, *Phys. Lett. B* **729**, 108 (2014).
- [9] G. Aarts, E. Seiler, D. Sexty, and I.-O. Stamatescu, *Phys. Rev. D* **90**, 114505 (2014).
- [10] M. Cristoforetti, F. DiRenzo, and L. Scorzato, *Phys. Rev. D* **86**, 074506 (2012).
- [11] H. Fujii, D. Honda, M. Kato, Y. Kikukawa, S. Komatsu, and T. Sano, *J. High Energy Phys.* **10** (2013) 147.
- [12] A. Roberge and N. Weiss, *Nucl. Phys.* **B275**, 734 (1986).
- [13] Y. Aoki, G. Endrödi, Z. Fodor, S. D. Katz, and K. K. Szabó, *Nature (London)* **443**, 675 (2006).
- [14] H. Kouno, Y. Sakai, K. Kashiwa, and M. Yahiro, *J. Phys. G* **36**, 115010 (2009).
- [15] P. de Forcrand and O. Philipsen, *Nucl. Phys.* **B642**, 290 (2002).
- [16] L.-K. Wu, X.-Q. Luo, and H.-S. Chen, *Phys. Rev. D* **76**, 034505 (2007).
- [17] M. D’Elia and M.-P. Lombardo, *Phys. Rev. D* **67**, 014505 (2003).
- [18] M. D’Elia and M.-P. Lombardo, *Phys. Rev. D* **70**, 074509 (2004).
- [19] P. de Forcrand and O. Philipsen, *Phys. Rev. Lett.* **105**, 152001 (2010).
- [20] K. Nagata and A. Nakamura, *Phys. Rev. D* **83**, 114507 (2011).
- [21] Y. Sakai, K. Kashiwa, H. Kouno, and M. Yahiro, *Phys. Rev. D* **77**, 051901 (2008).
- [22] Y. Sakai, T. Sasaki, H. Kouno, and M. Yahiro, *J. Phys. G* **39**, 035004 (2012).
- [23] Y. Sakai, K. Kashiwa, H. Kouno, M. Matsuzaki, and M. Yahiro, *Phys. Rev. D* **78**, 076007 (2008).
- [24] J. Sugano, J. Takahashi, M. Ishii, H. Kouno, and M. Yahiro, *Phys. Rev. D* **90**, 037901 (2014).
- [25] C. R. Allton, S. Ejiri, S. J. Hands, O. Kaczmarek, F. Karsch, E. Laermann, and C. Schmidt, *Phys. Rev. D* **68**, 014507 (2003).
- [26] S. Ejiri, Y. Maezawa, N. Ukita, S. Aoki, T. Hatsuda, N. Ishii, K. Kanaya, and T. Umeda (WHOT-QCD Collaboration), *Phys. Rev. D* **82**, 014508 (2010).
- [27] M. D’Elia, F. DiRenzo, and M. P. Lombardo, *Phys. Rev. D* **76**, 114509 (2007).
- [28] P. Cea, L. Cosmai, M. D’Elia, and A. Papa, *J. High Energy Phys.* **02** (2007) 066.
- [29] M. D’Elia and F. Sanfilippo, *Phys. Rev. D* **80**, 014502 (2009).
- [30] S. Borsanyi, G. Endrodi, Z. Fodor, S. D. Katz, S. Krieg, C. Ratti, and K. K. Szabo, *J. High Energy Phys.* **08** (2012) 053.
- [31] A. Ali Khan *et al.* (CP-PACS Collaboration), *Phys. Rev. D* **63**, 034502 (2000).
- [32] Y. Iwasaki, *Nucl. Phys.* **B258**, 141 (1985).

- [33] B. Sheikholeslami and R. Wohlert, *Nucl. Phys.* **B259**, 572 (1985).
- [34] A. Ali Khan *et al.* (CP-PACS Collaboration), *Phys. Rev. D* **64**, 074510 (2001).
- [35] Y. Maezawa, N. Ukita, S. Aoki, S. Ejiri, T. Hatsuda, N. Ishii, and K. Kanaya (WHOT-QCD Collaboration), *Phys. Rev. D* **75**, 074501 (2007).
- [36] P. Cea, L. Cosmai, M. D'Elia, and A. Papa, *Phys. Rev. D* **77**, 051501 (2008).
- [37] P. Cea, L. Cosmai, M. D'Elia, C. Manneschi, and A. Papa, *Phys. Rev. D* **80**, 034501 (2009).
- [38] P. Cea, L. Cosmai, M. D'Elia, and A. Papa, *Phys. Rev. D* **81**, 094502 (2010).
- [39] P. Huovinen and P. Petreczky, *Nucl. Phys.* **A837**, 26 (2010).
- [40] O. Philipsen and L. Zeidlewicz, *Phys. Rev. D* **81**, 077501 (2010).
- [41] A. Bazavov *et al.* (HotQCD Collaboration), *Phys. Rev. D* **85**, 054503 (2012).